World Academy of Science, Engineering and Technology
International Journal of Mechanical and Mechatronics Engineering
Vol:6, No:8, 2012

Enhancement of Impingement Heat Transfer on a Flat Plate with Ribs

M. Kito, M. Takezaki, T. Shakouchi, K. Tsujimoto, T. Ando

***Abstract*—**Impinging jets are widely used in industrial cooling systems for their high heat transfer characteristics at stagnation points. However, the heat transfer characteristics are low in the downstream direction. In order to improve the heat transfer coefficient further downstream, investigations introducing ribs on jet-cooled flat plates have been conducted. Most studies regarding the heat-transfer enhancement using a rib-roughened wall have dealt with the rib pitch. In this paper, we focused on the rib spacing and demonstrated that the rib spacing must be more than 6 times the nozzle width to improve heat transfer at Reynolds number $Re=5.0\times10^3$ because it is necessary to have enough space to allow reattachment of flow behind the first rib.

***Keywords*—**Forced convection, heat transfer, impinging jet cooling, rib roughened wall

I. Introduction

THE application of impinging jets for cooling, drying, and cleaning can be found in a wide variety of industries by virtue of their high heat and mass transfer on and around stagnation points. They are therefore a vital subject for many researchers in both the academic and industrial fields. R. Viskanta [1] provided detailed reviews of impingement heat transfer. Since the understanding of free jets is essential to reveal the mechanism of impinging jets and improve technical methods, the effects of nozzle configurations, jet velocity, and ambient conditions have been well addressed. Jet impingement has also been extensively studied, with investigations of how such parameters as single and multiple jets, nozzle and impingement wall configurations, and the angle between the jet and impingement wall affect the heat transfer performance. Investigations of the heat transfer performance of impinging jets on both convex and concave semi-circular surfaces were conducted [2] – [3] and showed the effect of curvature on the heat transfer and visualized flow characteristics. In order to obtain better heat transfer characteristics in the downstream, the use of multiple array jets or ribs, which is quite a common technique in channel flow [4] – [8], has been considered. In this paper, we arranged ribs on a heated flat plate, and the effects of the location of each rib on the heat transfer characteristics were examined.

M. Kito is an Assitant Professor at the Mechanical Engineering Department, Suzuka National College of Technology, Mie, Japan, on leave from the Graduate School of Engineering, Mie University, Mie, Japan (e-mail: kito@mech.suzuka-ct.ac.jp).

M. Takezaki was with the Control Engineering Department, Nara National College of Technology, Nara, Japan.

T. Shakouchi is a Professor at the Graduate School of Engineering, Mie University, Mie, Japan.

K. Tsujimoto is a Professor at the Graduate School of Engineering, Mie University, Mie, Japan.

T. Ando is an Assitant Professor at the Graduate School of Engineering, Mie University, Mie, Japan.

Some studies can be found regarding the heat transfer and flow characteristics of impinging jets along a rib-roughened wall. W. M. Chakroun, A. A. Abdel-Rahman, and S. F. Al-Fahed [9] found heat transfer augmentation when using an impingement plate of multiple square arrays. S. V. Ekkad and D. Kontrovitz [10] performed an experiment to study the heat transfer characteristics of circular jet impingement on a dimpled wall and concluded that the presence of dimples lowered the heat transfer compared to the case of channel flow. Augmentation of convective heat transfer to impinging jets using detached ribs was reported by V. Katti and S. V. Prabhu [11]. C. Gau and L. C. Lee [12] – [13] applied rectangular and triangular ribs on the impingement wall. They reported that a higher heat transfer coefficient could be obtained using triangular ribs than using rectangular ones because the triangular ribs encouraged the jet to flow smoothly to the wall and generate vortexes behind the ribs. Also, they varied the ratio of the rib height and nozzle width and varied the rib pitch. It was demonstrated that a lower ratio of rib height to nozzle width provided higher heat transfer. Despite theirs and other detailed studies, little attention has been given to the rib spacing. Most studies considering rib-roughened walls including channel flow deal with the rib pitch. That is, the spacing of the ribs is always same. This paper puts its focus on the rib spacing as a factor to improve the heat transfer characteristics of impinging jets, using relatively large ribs.

The experiments were divided into two parts. The first experiment was conducted with one rib on the wall to demonstrate the effects of the rib location and the nozzle−wall distance. The normalized nozzle−wall distance was changed from 5 to 20 and the normalized rib location was changed from 0 to 8. The second experiment presented the optimum rib locations using several ribs. Both experiments were conducted at Reynolds number $Re=5.0\times10^3$ based on the nozzle exit width B=5 mm and the jet exit velocity.

II. Experimental Apparatus And Procedure

An experimental investigation was carried out to study the on the heat transfer characteristics on the rib-roughened wall. The entire experimental set-up is sketched in Fig. 1. After the flow rate and air temperature were controlled by the valve and the air, the air ejects from the nozzle into ambient air with a temperature that was kept constant with the jet temperature within ± 0.3 ºC during the measurements. A nozzle was placed perpendicular to the impingement plate.

Fig. 2 shows a schematic diagram of the test section to measure the temperature distributions on the impingement plate. The impingement plate is made of a Bakelite plate 10 mm in thickness. Direct heating of a thin (40-μm) stainless steel foil attached to the plate done electrically with a uniform heat flux adjusted by a slide trance.

The net heat amount was calculated considering the heat transfer rate to the plate and the thermal radiation from the foil surface. The conduction and thermal radiation heat transfer were approximately 3% during a typical experiment. A total of 38 thermocouples (C-A) were placed 4 mm apart on the back side of the foil to measure the temperature distributions on the plate simultaneously by a data logger within 0.1°C accuracy. Ribs with square cross-section of 3 mm per side were applied to the stainless steel foil. The ribs were made of adiabatic material, so no significant heat could be transferred to the ribs. A nozzle was set perpendicular to the heated plate. The flow rate of the jet and the air temperature were controlled by a valve and cooler.

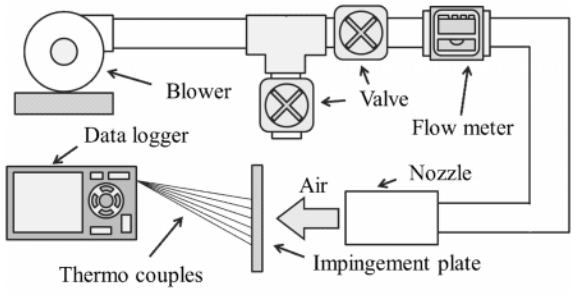

Fig. 1 Experimental set-up

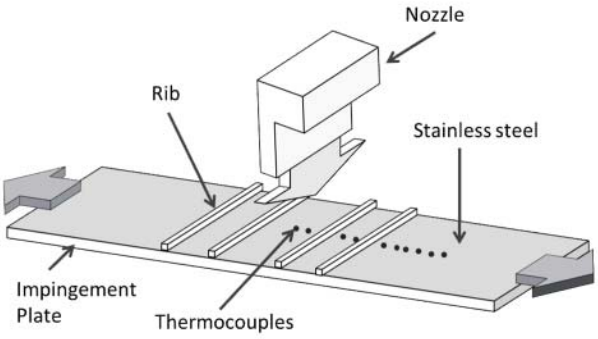

Fig. 2 Schematic diagram of the rib wall

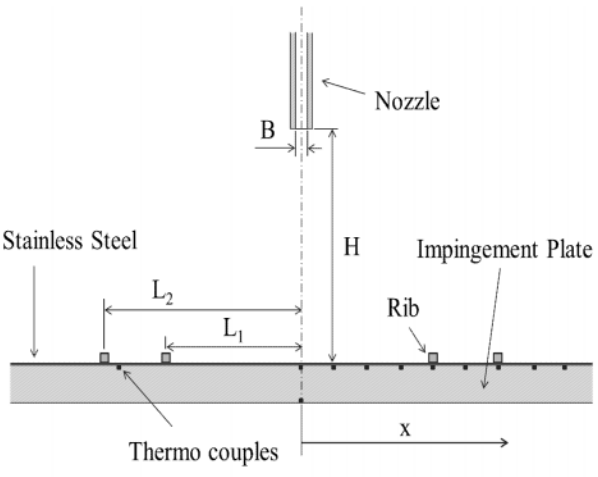

Fig. 3 Coordinate system

During the experiment the air issued from the nozzle to the plate. The nozzle used in this experiment had a rectangular exit area 5 mm × 100 mm, giving it an aspect ratio of 20.

The local heat transfer coefficient was calculated from the temperature distribution along the x axis using the thermocouples on the back side of the plate and the jet flow temperature as shown in (1). H. Martin [14] defined the entrainment factor as the temperature ratio between the jet-ambient and the jet-impinging plate surface, the value of which affects the heat transfer reduction. The jet temperature in all cases was controlled carefully to keep constant within $\pm 0.3^{\circ}C$ of the atmospheric temperature. Thus, the effect of entrainment claimed by H. Martin [14] could be neglected. In the estimation of the heat flux, to obtain the heat transfer rate, the heat loss due to thermal conduction into the impinging plate and thermal radiation from the surface were considered. The heat loss due to thermal conduction was estimated by the difference of the plate inner temperature and the impinging plate surface temperature.

$$h = \frac{Q}{A(T - T_{\infty})} \tag{1}$$

Where Q is the net heat amount considering the heat transfer rate to the plate and the thermal radiation, A is the smooth impingement wall area, T is the impingement wall temperature measured by the thermocouples, and T_{∞} is the room temperature.

The mean heat transfer coefficient $\bar{h}$ was defined as shown in (2).

$$\bar{h} = \frac{1}{A}\int h(x)dx \tag{2}$$

Where x is the distance from the stagnation point

The local Nusselt number was defined as follows:

$$Nu = \frac{h \cdot d}{\lambda} = \frac{Q \cdot D_h}{\lambda_a \cdot A(T - T_{\infty})}, \tag{3}$$

Where λ_a is the air thermal conductivity and the characteristic length is the hydraulic diameter.

Fig. 3 shows the detailed test section and coordinate system. The x axes starting at the stagnation point on the impingement wall increase in the streamwise direction. The normalized nozzle–wall distance H/B (H: nozzle–wall distance, B: nozzle width) was changed from 5 to 20 for one rib setting to find out the optimum rib location. The first rib was located L_1 from the stagnation point. After determining the optimum rib location, we arranged the second ribs symmetrically on the impingement wall L_2 from the stagnation point.

Flow visualization was also performed to observe the flow behavior along the rib-roughened wall. Air jets seeded homogenously using a W-515 fog machine (ANTARI) issued from the nozzle into the still fluid. The images of vortex structures were recorded with a digital video camera by illuminating the flow in the middle plane using a xenon light sheet. The flow visualization was conducted in a dark room to maintain the same conditions throughout the experiments.

III. EXPERIMENTAL RESULTS AND DISCUSSION

In order to investigate the nozzle properties, the free jet velocity was measured without the impingement plate. The normalized centerline velocities u/u_{max} (u_{max} is the maximum/ initial velocity at the nozzle exit) of the nozzle at Re=15,000 are shown in Fig. 4. The centerline velocity remained almost constant from the nozzle exit up to x/D_h =1.7 where D_h is the hydraulic diameter. J. N. B. Livingood and P. Hrycak [15] suggested that the potential core length should be taken as the distance from the nozzle exit where the jet velocity decays to 95% of its maximum. Thus, the potential core of this nozzle was found to be x/D_h= 2.5 in accordance with their suggestion.

Thereafter, the velocity decayed with $u/u_{max} \propto (x/D_h)^{-0.5}$ in the fully developed region, which is the empirical equation in the fully developed region for a rectangular nozzle. It is clear that the centerline velocity profile is remarkably well fitted by the distinctive equation, which confirms the reliability of the nozzle used in the presented experiment.

Fig. 5 shows the mean velocity distribution at the nozzle exit to understand the property of the nozzle. The profile was found to be nearly a top-hat, at least at the center. The velocity distribution at the center varies less than 5%.

First, the heat transfer experiments on a smooth surface were conducted in order to understand the heat transfer chacteristics on the impingement plate for comparison purposes. Fig. 6 illustrates the local Nusselt number (*Nu*) distribution on the smooth-surfaced impingement wall (i.e., without ribs) at *H/B*=15. The local Nusselt number was calculated by using (3) as mentioned before. Since the temperature was distributed symmetrically, the calculated *Nu* was also distributed symmetrically. Thus, the distribution on only one side is presented in Fig. 6. The horizontal axis presents the distance from the stagnation point normalized by the nozzle exit width *B*. We use *B*, not D_h, to normalize so that the position can be easily recognized. The maximum for *Nu* was obtained near the stagnation point due to the high impinging jet velocity, and *Nu* decreased rapidly downstream. At *x*/B=8, *Nu* decayed to half of the maximum value at the stagnation point.

The stagnation *Nu* when a rectangular nozzle jet impinges for the Reynolds number based on the nozzle width (Re_B) from 1×10^4 to 2×10^5 was evaluated as follows [16].

$$Nu_B = 1.42 \cdot \Pr^{0.43} \cdot \mathrm{Re}_B^{0.58} \cdot (H/B)^{-0.02} \quad (4)$$

The stagnation *Nu* was 65.3 in Fig. 5 and Nu_B=61.3 was obtained from (4).

Good agreement of about 6.7% was achieved for the impingement cooling characteristics. Next, the heat transfer experiments on the rib roughened wall were conducted. In the following section, the effects of one rib will be described on various rib locations.

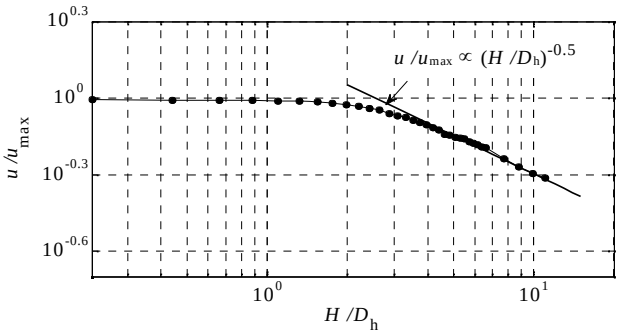

Fig. 4 The centerline velocity at Re=15000

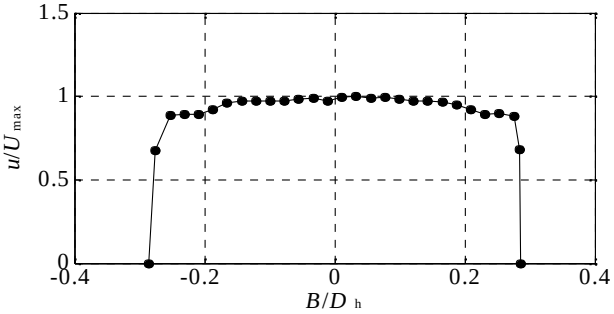

Fig. 5 The mean velocity

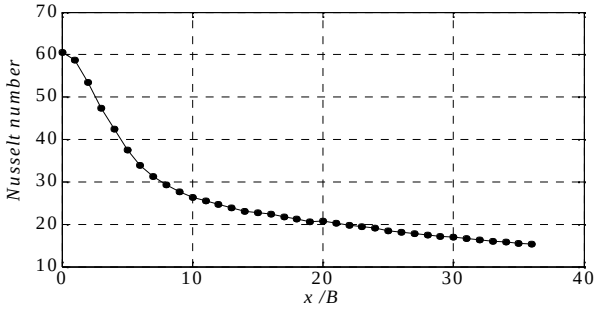

Fig. 6 The local Nusselt number without a rib at *H/B*=15

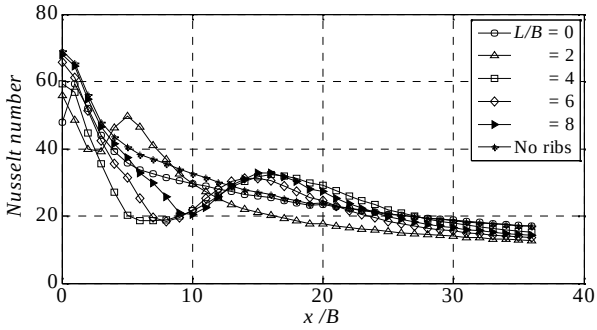

(a) *H/B* = 5

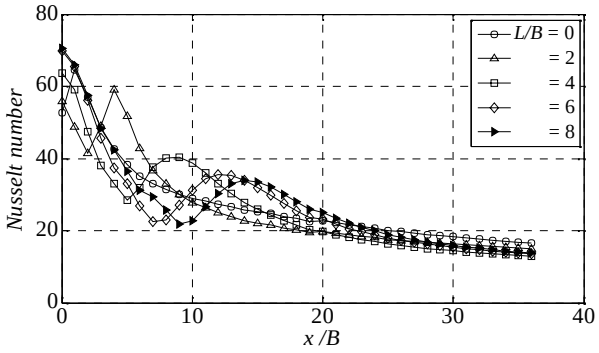

(b) H/B = 10

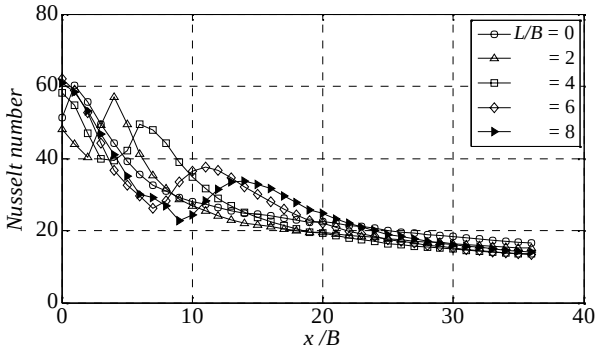

(c) H/B = 15

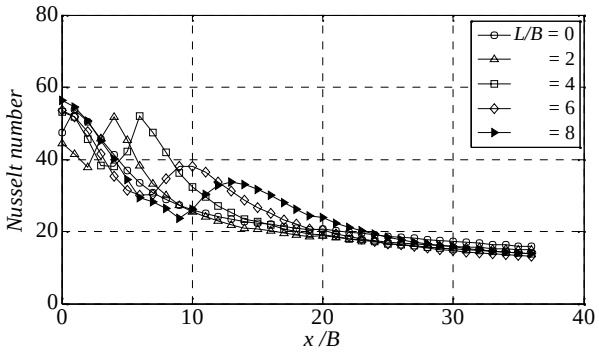

(d) H/B = 20

Fig. 7 Nusselt number distribution with single rib

Figs. 7(a)–(d) show the local Nusselt number with one rib at L_1/B=0–8. The distributions were plotted only on one side since they were symmetric. It should be noted that the results for H/B=10–20 show the same trend. Fig. 7(a) indicates that a second peak caused by the rib appears a distance from the rib in comparison with the others owing to the high impinging jet velocity. Because of the high impinging velocity, the flow after impingement bounces back and the flow rate is not sufficient to promote the heat transfer along the wall. Similar distributions are observed at $H/B \geq 10$ and the maximum heat transfer at the second peak is about 20% larger than that at the stagnation point.

In the case of L_1/B=0, the local heat transfer appears low since the jet impinges the rib at the stagnation point; however, it shows a rise to the maximum behind the rib and decays gradually downstream. A maximum local heat coefficient occurs at the stagnation point and the local minimal and local maximum values occur at the rib and behind the rib except for the case of L_1/B=0. Although the second peak behind the rib increases at maximum about 20% more than that at the stagnation point, the local heat transfer at the stagnation point is much lower than that without a rib.

In the case of L_1/B=2, the second peak occurs at x/B=4–5 regardless of the nozzle−wall distance. In comparison with the result shown in Fig. 11, after impingement the jet separates from the rib edge in the downstream rather than the upstream, and reattaches to the wall at x/B=4–5, since the jet width before impingement was $L/B \cong 2$.

In the case of L_1/B=4–8, the second peak increases and the location of the second peak becomes closer to the rib as H/B increases. This explains that the higher H/B, the smaller bounce back produces on the impingement wall.

Fig. 8 describes the local Nusselt number at the stagnation point (Nu_s) normalized by the local Nusselt number without ribs (Nu_n) versus the normalized nozzle−wall distance for various rib locations. The normalized nozzle−wall distance H/B ranged from 5 to 20, and the normalized rib location (L_1/B) ranged from 0 to 8. The equivalence L_1/B=0 means that the rib location coincides with the stagnation point. The Nusselt number ratio shows L_1/B=6, 8 > 4 > 0, 2 with no dependency of the nozzle−wall distance. The Nusselt number at L_1/B=6, 8 provides almost the same value at that without a rib. It is therefore concluded that there is no effects of the rib at L_1/B=6; however, the observed the Nusselt number at L_1/B<6 becomes low. This result must be attributed to the flow block caused by locating the rib near the stagnation point. The Nusselt number at L_1/B=0 is 30% smaller than the others at most.

Fig. 9 shows the mean Nusselt number ($\overline{Nu}$) along the impingement plate x/B=0–15 normalized by the mean Nusselt number without ribs ($\overline{Nu}_n$) versus the normalized nozzle−wall distance for various rib locations.

At all nozzle−wall distances, a similar behavior could be observed.

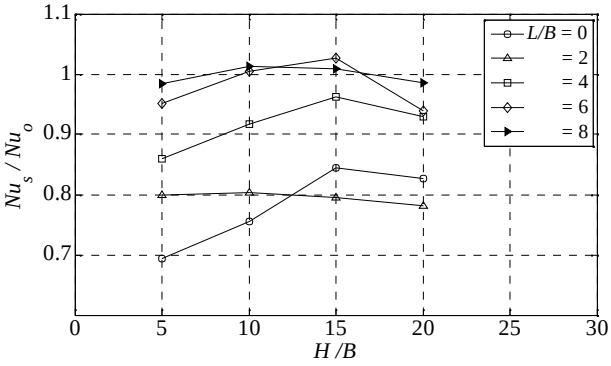

Fig. 8 Nusselt number at the stagnation point

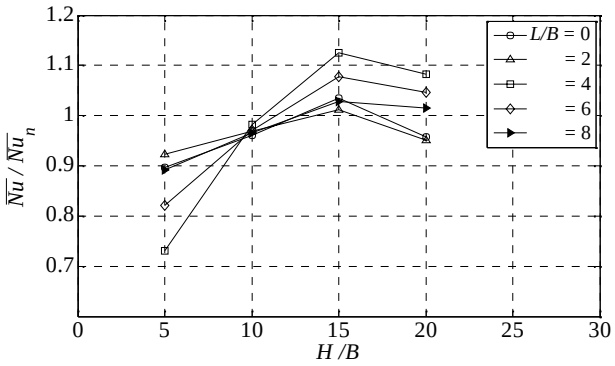

Fig. 9 Mean Nusselt number

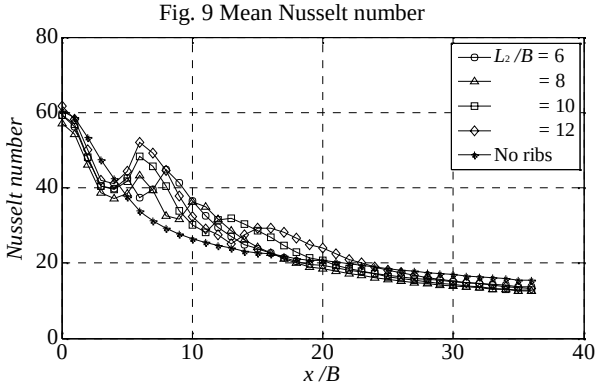

Fig. 10 Nusselt number distribution at H/B=15, L_1/B=4

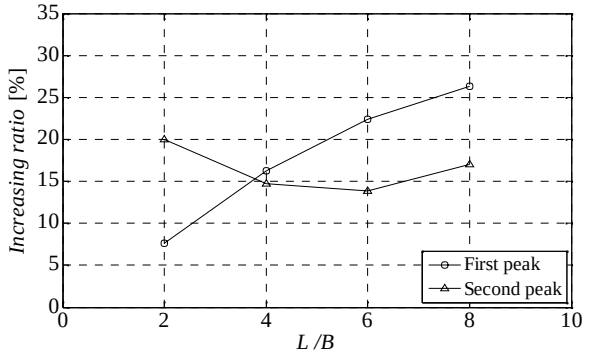

Fig. 11 Increasing heat transfer ratio at H/B=15, L_1/B=4

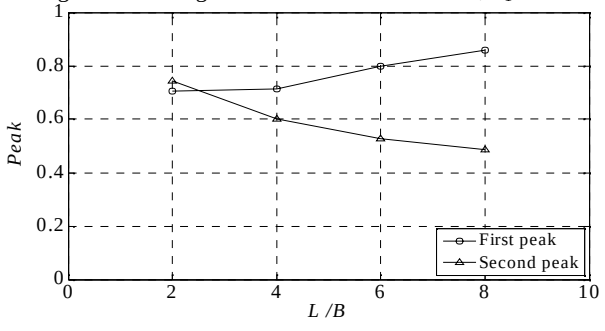

Fig. 12 Normalized peak value at H/B=15, L_1/B=4

The minimum normalized mean heat transfer coefficient occurred at H/B=5 and maximum at H/B=15. At H/B=5, the flow simply bounced back after the impingement due to its high impinging velocity.

Thus, the flow along the wall has no more momentum to improve the heat transfer. At H/B=15, on the contrary, the flow decays before impingement and has a low momentum downstream. The results indicate that the optimum rib location is L_1/B=4 at H/B=15, at which the mean heat transfer coefficient increases about 10% compared with that without a rib. In the following section, the effects of multiple ribs will be described by reference to the previous section in which the results indicated that the optimum rib location was L_1/B =4 at H/B=15. Therefore, while one rib was arranged at L_1/B =4 and the nozzle−wall distance was constant H/B=15, the second ribs were located symmetrically on the impingement wall L_2 from the stagnation point. The L_2/B was changed from 6 to 12. The results are presented in Fig. 10.

The second peak for L_2/B=6 was quite low compared with that of the other conditions. Because of the narrow spacing between ribs, the flow was discouraged from reattaching on the impingement wall. In the same way, the second peak for L_2/B=8 was not remarkable. On the contrary, in the case of L_2/B=10 and 12, the second peak behind the first rib reached the same level as that without the second ribs. Therefore, in order to regain adequate heat transfer behind a rib due to the flow reattachment, the rib spacing has to be more than 6 times the nozzle width. The mean Nusselt number over x/B=0–15 for L_2/B=12 was about 15% more than that without ribs. Fig. 11 indicates the increasing heat transfer ratio (Nusselt number) of the local maximum value behind the rib and the local minimal value around the rib. A greater spacing between ribs resulted in an increased heat transfer ratio for the first peak as the L_2/B increased. However, that for the second peak seemed somewhat constant at about 0.25.

Fig. 12 describes the peak value of the local Nusselt number normalized by the local Nusselt number at the stagnation point (Nu_0). The first peak increased and the second peak decreased as the L_2/B increased. As mentioned above, the first peak increased because a large L_2/B provided sufficient space to allow reattachment behind the first rib. There is no doubt that ribs remarkably affect the heat transfer characteristics; however, the increasing ratio of the second peak and the local minimal value of the heat transfer coefficient was found to be more or less constant in Fig. 11.

Therefore, the second peak decreases because the heat transfer coefficient at the second rib, which coincides with the local minimal value of the heat transfer coefficient, is not enough to regain adequate heat transfer behind the second rib. Accordingly, there would be little enhancement of the heat transfer even if more ribs were arranged in the downstream.

The vortex structures of the impinging jets were visualized by the tracer method, and the effects of the ribs on the wall were examined at Reynolds number 200. The results in the middle plane are shown in Fig. 13. Figs. 13 (a)–(f) show the jet flow behavior when a rib is arranged at the stagnation point, at L_1/B=0, 2, 4, 6, 8, and at L_1/B=4 and L_2/B =12, respectively. Because the ribs were transparent, it was a little difficult to recognize the ribs. Closed square marks in Fig. 12 indicate the ribs.

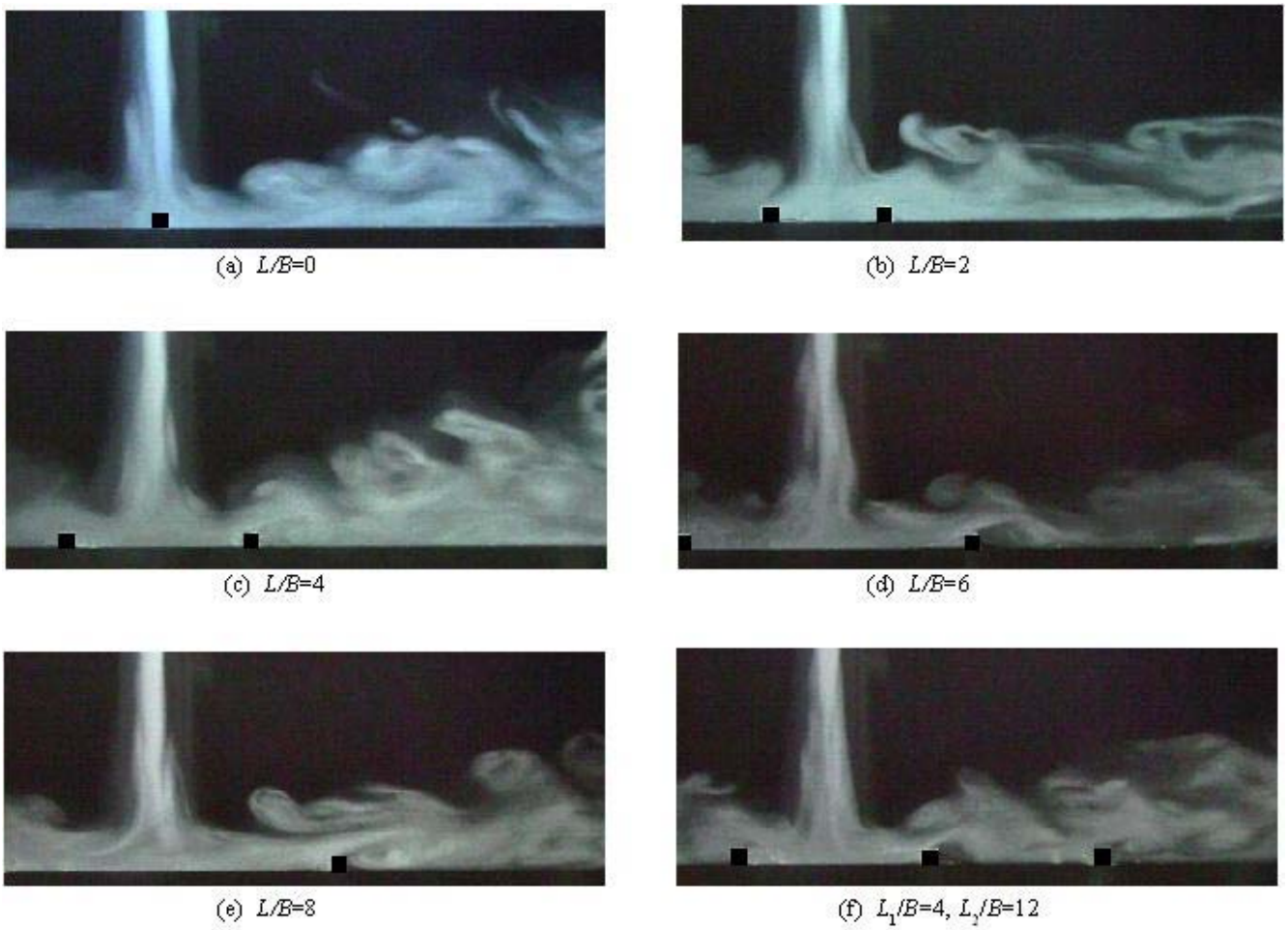

Fig. 12 Flow visualizations at *H/B*=15

Fig. 13 shows that the jet width before the impingement expands to *L/B* ≅ 2. Figs. 13 (a) and (b) yield no indisputable separation at the rib edge. However, a vortex moving along the wall can be clearly seen. On the other hand, Figs. 13 (c) and (d) clearly show the separation at the rib edge and reattachment downstream. It is clear that the rib creates a recirculation region and the vortex moves along the wall. A similar phenomenon can be seen in Fig. 13 (f) with multiple ribs. The separation and reattachment regions produced by each rib are observed. These distinct regions improve the heat transfer characteristics on the impingement wall mentioned in Fig. 9. In this respect, the visualized images confirm the results from the heat-transfer experiments.

IV. Concluding Remarks

This study examined the effects of impingement-wall rib spacing on flow and heat transfer characteristics. The main results obtained were:

- The normalized nozzle−wall distance H/B was changed from 5 to 20 and rib location L1/B was changed from 0 to 8. A high heat transfer coefficient was obtained at H/B=15, L1/B=4 when only one rib was placed on the impingement wall.
- When a second rib was placed on the impingement wall, it was found that the rib spacing had to be more than 6 times the nozzle width to improve heat transfer because it is necessary to create enough space to allow reattachment of the flow behind the first rib. The first peak increases and the second peak decreases as the L2/B increases. The mean heat transfer coefficient over x/B=0–15 for L2/B=12, L1/B=4 at H/B=15 was about 15% more than that without ribs.
- The flow visualization demonstrated the effects of the rib location on the flow characteristics of the impinging jet and supported the results of the heat-transfer experiments.

ACKNOWLEDGMENT

This study was supported by a research grant from the Foundation for Applied Research and Technological Uniqueness at N.U.T.

REFERENCES

[1] R. Viskanta, "Heat transfer to impinging isothermal gas and flame jets," Exp. Thermal and Fluid Science, vol.6, 1993, pp.111–134.
[2] T.L.Chan, Y.Zhou, M.H.Liu, C.W.Leung, "Mean flow and turbulence measurements of the impingement wall jet on a semi-circular convex surface," Experiments in Fluids 34, 2003, pp.140-149.
[3] C.Gau and C.M. Chung, "Surface curvature effect on slot air-jet impingement cooling flow and heat transfer process," ASME J. of Heat Transfer 113, 1991, pp.858-864.
[4] R.L.Webb, E.R.G.Eckert, R.J. Goldstein, "Heat transfer and friction in tubes with repeated-rib roughness," Int. J. Heat Mass Transfer, vol.14, 1971, pp.601–617.
[5] J.C.Han, L.R. Glicksman, W.M. Rohsenow, "An investigation of heat transfer and friciton fro rib-roughened surfaces," Int. J. Heat Mass Transfer, vol.21, 1978, pp.1143–1156.
[6] E.M.Sparrow, W.Q. Tao, "Enhanced heat transfer in a flat rectangular duct with streamwise-periodic disturbances at one principal wall," Trans. ASME J. Heat Trans., vol.105, 1983, pp.851–861.
[7] T.M. Liou, J.J. Hwang, "Effect of ridge shapes on turbulent heat transfer and friction in a rectangular channel," Int. J. Heat Mass Transfer., vol.36, 1993, pp.931–940.
[8] S. Okamoto, S. Seo, K. Nakaso, I. Kawai, "Turbulent shear flow and heat transfer over the repeated two-dimensional square ribs on ground plane," Trans. ASME J. Fluids Eng., vol.115, 1993, pp.631–637.
[9] W.M. Chakroun, A.A. Abdel-Rahman, S.F. Al-Fahed, "Heat transfer augmentation for air jet impinged on a rough surface," Appl. Therm. Eng. vol.18, 1998, pp.1225-1241.
[10] S.V. Ekkad and D. Kontrovitz, "Jet impingement heat transfer on the dimpled target surfaces," Int. J. Heat Fluid Flow vol.23, 2002, pp.22-28.
[11] V. Katti and S.V. Prabhu, "Heat transfer enhancemnet on a flat surface with axisymmetric detached ribs by normal impingement of circular air jet," Int. J. Heat Fluid Flow vol.29, 2008, pp.1279-1294.
[12] C. Gau and L.C.Lee, "Impingement cooling flow structure and heat transfer along rib-roughened walls," Int. J. Heat Mass Transfer, vol.35, 1992, pp.3009-3020.
[13] C. Gau and L.C.Lee, "Flow and impingement cooling heat transfer along triangular rib-roughened walls," Int. J. Heat Mass Transfer, vol.43, 2000, pp.4405-4418.
[14] H. Martin, "Heat and mass transfer between impinging gas jets and solid surface," Adv. Heat Transfer, vol.13, 1977, pp.1-60.
[15] J. N. B. Livingood and P. Hrycak, "Impingement Heat Transfer from Turbulent Air Stream Jets to Flat Plate," A literature survey, NASA TM X-2778, 1973.
[16] JSME Data Book; Heat Transfer 5th Edition, 2009 , pp.39-51